

Effect of Pore Confinement of NaNH_2 and KNH_2 on Hydrogen Generation from Ammonia

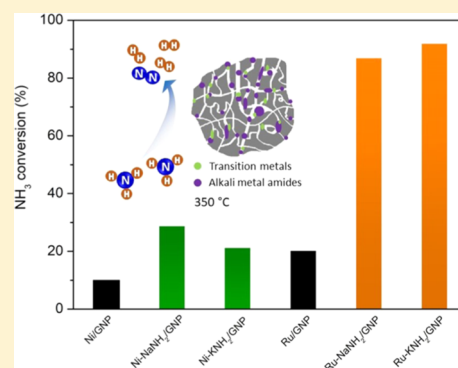
Fei Chang,[†] Han Wu,[‡] Robby van der Pluijm,[†] Jianping Guo,[‡] Peter Ngene,^{*,†} and Petra E. de Jongh^{*,†}

[†]Inorganic Chemistry and Catalysis, Debye Institute for Nanomaterials Science, Utrecht University, Universiteitsweg 99, 3584 CG Utrecht, The Netherlands

[‡]Dalian National Laboratory for Clean Energy, Dalian Institute of Chemical Physics, Chinese Academy of Sciences, 116023 Dalian, P. R. China

S Supporting Information

ABSTRACT: The development of efficient catalysts for hydrogen generation via ammonia decomposition is crucial for the use of ammonia as an energy carrier. Here, we report the effect of pore confinement of NaNH_2 and KNH_2 on ammonia decomposition catalysis. For the first time, Ni- or Ru-doped NaNH_2 and KNH_2 were confined in carbon nanopores using a combination method of solution impregnation and melt infiltration. Structure characterization indicates the nanoscale intimacy between transition metals and alkali metal amides inside the pores of the carbon support. As a result, 8 wt % Ni-doped NaNH_2 and KNH_2 nanocomposites give NH_3 conversions of 79 and 60%, respectively at 425 °C, close to the performance of a 5 wt % Ru/C reference catalyst. 0.8 wt % Ru-doped nanocomposites exhibit even better catalytic performance, with about 95% NH_3 conversion at a moderate temperature of 375 °C. The hydrogen production rates of these Ni- and Ru-doped nanocomposites in a pure NH_3 flow are about 3–4 times higher than for the recently reported novel catalysts such as Ni– Li_2NH and Ru– $\text{Li}_2\text{NH}/\text{MgO}$. Interestingly, the apparent activation energies of the Ru- or Ni-based catalysts decrease 20–30 kJ mol^{−1} by co-confinement with alkali metal amides. The strategy of nanoconfinement of alkali metal amides in porous hosts may open a new avenue for effectively generating H_2 from NH_3 at low temperatures.



1. INTRODUCTION

The general concern about the CO_2 emissions associated with the utilization of fossil fuels has led to an interest in developing sustainable energy. The use of hydrogen produced directly or indirectly from renewable energy sources such as solar light or wind is an attractive option.^{1,2} However, the potential of the “hydrogen economy” is currently limited by the challenge of storing hydrogen in a safe and economical manner.^{3,4} A wide range of hydrogen storage materials such as metal alloys, complex metal hydrides, and borohydrides have been explored, but none of them can meet the target of the US Department of Energy for practical applications.⁵ Ammonia is considered as a suitable hydrogen carrier, despite its toxicity, because of its high energy density (4 kWh kg^{−1}), high hydrogen content (17.7 wt %), and well-developed storage and transportation technology.^{6,7} Ammonia decomposition can provide hydrogen for fuel cells on-site without CO_x impurities.^{8,9} Therefore, the development of catalytic systems capable of releasing hydrogen from ammonia, especially catalysts that can work at low temperatures, has received much attention.¹⁰

In the last two decades several catalysts, including transition metals (TMs), alloys, carbides, and nitrides, have been investigated for ammonia decomposition.^{11–18} Among the systems studied so far, Ru was found to be the most active

metal, followed by Ir, Rh, Ni, Pt, Pd, and Fe.⁶ Xu et al. conducted a systematic investigation of the support effect of Ru-based catalysts on ammonia decomposition, and found that, under the same conditions, carbon nanotube (CNT)-supported Ru catalysts have better activities than those supported on AC, MgO, ZrO_2 , Al_2O_3 , and TiO_2 .¹⁹ Recent works showed that graphitic carbon supports such as graphene and N-doped nanocarbon tubes or fibers are beneficial for the recombinative desorption of surface nitrogen atoms.^{20,21} Alkali metal oxides or hydroxides are effective promoters with increasing promotion efficiency $\text{Li} < \text{Na} < \text{K} < \text{Cs}$, although the promoting mechanism is still being debated.^{22,23} Many studies focused on Ni rather than Ru catalysts because of the lower cost of Ni.¹⁶ The catalytic performance of NH_3 decomposition over Ni catalysts is strongly dependent on their microstructure, active sites, and the texture of supports.^{24,25}

Another interesting class of catalysts is those based on alkali metal amides or imides. In 1894, Titherley observed that NaNH_2 can produce Na, N_2 , and H_2 in a flow of NH_3 .²⁶ David

Received: April 25, 2019

Revised: July 25, 2019

Published: August 12, 2019

Table 1. List of Samples Prepared in This Work^a

sample	transition metal loading (wt %)	alkali amide loading (wt %)	sample	transition metal loading (wt %)	alkali amide loading (wt %)
GNP			Ni/GNP–KNH ₂ –PM	8	20
Ni/GNP	10		Ru/GNP	5	
NaNH ₂ /GNP		20	Ru–NaNH ₂ /GNP	0.1–1.6	5–30
KNH ₂ /GNP		20	Ru–KNH ₂ /GNP	0.1–1.6	5–30
Ni–NaNH ₂ /GNP	8	20	Ru–NaOH/GNP	5	
Ni–KNH ₂ /GNP	8	20	Ru–KOH/GNP	5	
Ni/GNP–NaNH ₂ –PM	8	20			

^aAll of the weight loadings shown in this table are nominal loadings.

et al. found that NaNH₂ was active for NH₃ decomposition when tested in a stainless steel reactor.²⁷ A more recent development is the use of composites of lithium imide and transition metals (nitrides). Guo et al. reported that Li₂NH combined with 3d transition metals or their nitrides leads to high catalytic activities for NH₃ decomposition, with the MnN–Li₂NH composite having an activity similar to that of 5 wt % Ru/CNTs.^{28,29} They postulated that the imide and transition metal nitride first formed a ternary nitride intermediate evolving hydrogen in the process; and then the intermediate reacted further with ammonia to yield nitride, imide, and nitrogen. It was proposed that the ternary nitride intermediate helped to stabilize the transition metal–N bond and thus decrease the kinetic barriers. However, Ru is not known to form stable ternary nitrides with Li. Theoretical research suggests that a strong repulsive force between negatively charged NH_x ($x = 1, 2$) species in Li₂NH hinders the NH_x coupling and decomposition to form N₂ and H₂. However, in the presence of Ru, the electron transfer from Ru to Li₂NH decreases this repulsion and thus the kinetic barrier, hence, facilitating the NH_x coupling and decomposition of Li₂NH or LiNH₂ to produce N₂ and H₂.³⁰ These transition metal–amide composites were mostly prepared by high energy ball milling. The fact that this method leads to relatively large crystallites and a not very well defined morphology hinders the improvement of ammonia decomposition performance and complicate a detailed understanding of the catalytic mechanism.

Solution impregnation and melt infiltration are effective methods for the preparation of supported catalysts, and have also been explored for carbon-supported nanoparticles of light metal hydrides or amides, such as MgH₂, NaAlH₄, LiH, and LiNH₂.³¹ Pore confinement and nanosizing can increase the hydrogen desorption/absorption rates of metal hydrides and amides.³² Recently, we showed that carbon-supported Ni–LiNH₂ composites are promising for the storage and decomposition of ammonia.³³ The Ni–LiNH₂/C composite was synthesized via solution impregnation of the carbon with Ni and Li precursors. However, this method only achieved 44% LiNH₂ in the pores of carbon xerogels, thus presenting large crystallites of LiNH₂. On the other hand, to the best of our knowledge, successful nanosizing or nanoconfinement of the analogues of LiNH₂ (i.e., NaNH₂ and KNH₂) and their catalytic applications have not yet been reported.

In this work, we report a simple method to achieve nanoconfinement of NaNH₂ and KNH₂ using a graphite nanoplatelet (GNP) as support. Structure characterization revealed that NaNH₂ and KNH₂ with particle sizes of 2–10 nm were efficiently confined inside the pores of the carbon support. We show that the pore confinement of NaNH₂ and

KNH₂ together with transition metal nanoparticles (Ni or Ru) has a remarkably beneficial effect on hydrogen generation via decomposition of ammonia.

2. EXPERIMENTAL SECTION

All experiments were performed at Utrecht University unless stated otherwise.

2.1. Materials. All chemicals were stored in an argon-filled glovebox (O₂ < 1 ppm, H₂O < 1 ppm). Graphite nanoplatelets (denoted as GNP) with a specific surface area of 500 m² g^{−1} were obtained from Imerys Graphite and Carbon (formerly known as Timcal) Switzerland. GNP was dried at 550 °C for 6 h under an argon flow before storing in the glovebox. NaNH₂ (95%, purity), metallic potassium (99%), anhydrous citric acid (99.5%), Nickel(II) nitrate hexahydrate (99%), sodium hydroxide (99%), potassium hydroxide (99%), and ruthenium(III) acetylacetonate (99.5%) were purchased from Sigma-Aldrich. KNH₂ powder was prepared by treating metallic potassium with NH₃ at room temperature for one week.

2.2. Catalyst Preparation. An overview of all samples and their transition metal and alkali amide loadings are given in Table 1.

Ni/GNP catalysts were prepared according to a previously reported procedure.³³ Nickel(II) nitrate hexahydrate and citric acid with a molar ratio of 3:2 were dissolved in demineralized water. GNP was impregnated with the volume of precursor solution equivalent to its pore volume, followed by drying under vacuum at 120 °C overnight. Then, the dried sample was reduced under a 10% H₂/N₂ flow at 350 °C with a ramp rate of 2 °C min^{−1} for 1 h.

For the preparation of Ru/GNP catalysts, the relevant amounts of ruthenium(III) acetylacetonate were dissolved in acetone. GNP was impregnated with a volume of precursor solution equivalent to its pore volume, followed by drying under vacuum for 2 h at 90 °C. The dried samples were reduced under a 10% H₂/Ar flow at 350 °C with a ramp rate of 2 °C min^{−1} for 1 h.

Ru–NaOH/GNP and Ru–KOH/GNP catalysts were prepared by wetness incipient impregnation of Ru/GNP with aqueous solutions of NaOH or KOH. After impregnation, the samples were dried under vacuum for 2 h at 90 °C and reduced under a 10% H₂/Ar flow at 350 °C with a ramp rate of 2 °C min^{−1} for 1 h. The atomic ratios of Na or K to Ru in the catalysts were 2:1, where the maximum promotional effect was observed.³⁴

The NaNH₂/GNP nanocomposite was prepared by melt infiltration. The relevant amounts of NaNH₂ powder were mixed with GNP in a mortar, placed in a graphite sample holder, and placed into a stainless steel autoclave. The autoclave was pressurized with 8 bar of NH₃, heated to 230

°C and held for 0.5 h. After cooling down to room temperature, the NH_3 pressure was released and purged with argon. The sample was stored in the glovebox and denoted as NaNH_2/GNP . The KNH_2/GNP nanocomposite was prepared in the same manner except for the heating program, with the samples being heated to 300 °C with a dwell time of 2.5 h.

Similarly, $\text{Ni-NaNH}_2/\text{GNP}$, $\text{Ni-KNH}_2/\text{GNP}$, $\text{Ru-NaNH}_2/\text{GNP}$, and $\text{Ru-KNH}_2/\text{GNP}$ nanocomposites were prepared by melt infiltrating pre-prepared Ni/GNP or Ru/GNP with NaNH_2 or KNH_2 , respectively.

Physical mixtures (denoted as $\text{Ni/GNP-NaNH}_2\text{-PM}$ and $\text{Ni/GNP-KNH}_2\text{-PM}$) were prepared by thoroughly mixing Ni/GNP and NaNH_2 or KNH_2 powder in a mortar in the glovebox.

2.3. Catalyst Characterization. X-ray diffraction (XRD) patterns were obtained at room temperature from $2\theta = 10$ to 80° with a Bruker AXS D8 Advance X-ray diffractometer instrument using $\text{Co K}\alpha$ radiation with a wavelength of 1.79026 Å. An air-tight sample holder was used to prevent air exposure. N_2 physisorption measurements were performed at -196°C using a Micromeritics Tristar 3000 apparatus. The BJH pore size distributions and mesopore volumes of the samples were determined from the adsorption branch of the isotherm. Micropore volumes were calculated using the t -plot method. Scanning electron microscopy–energy-dispersive X-ray spectroscopy (SEM–EDX) was performed using an FEI XL30 FEG SEM instrument in the secondary electron mode. Samples were placed on a conducting carbon film on the sample holder and coated with a platinum layer before measurements. Transmission electron microscopy (TEM) images were obtained using a Tecnai 20FEG (FEI) microscope with a field emission gun operated at 200 kV. High-angle annular dark-field scanning transmission electron microscopy (HAADF–STEM) and energy-dispersive X-ray spectroscopy (EDX) images were obtained from a TALOS F200X (FEI) electron microscope equipped with a field emission gun, a Fischione HAADF detector, and a SuperX EDX system. The samples were deposited onto the carbon grids inside the argon-filled glovebox and transferred to the microscope in an air-tight sample holder. 100 particles were counted for the statistics of particle size distributions of Ni and Ru catalysts. Thermogravimetric analysis (TGA) measurements were performed on a Netzsch 449C TG unit inside the glovebox at the Dalian Institute of Chemical Physics. Sample loading was about 5 mg. Argon was used as the carrier gas and the ramp rate was 5°C min^{-1} . X-ray absorption spectroscopy (XAS) measurements were conducted at the Dutch-Belgian beamline (DUBBLE) of the European Synchrotron Radiation Facility (ESRF) in Grenoble, France. The measurements were performed at the Ru K-edge (22117 eV) using a Si(111) crystal monochromator. The spectra of the $\text{Ru-KNH}_2/\text{GNP}$ and the Ru/GNP were collected in the fluorescence mode using a nine-element Ge detector, whereas the spectrum of the Ru foil was collected in the transmission mode using ionization chambers. Spectra analysis was conducted using the Athena and Artemis software package. The spectra energy was calibrated to the first inflection point of a metallic Ru foil in the derivative spectrum. The $\text{Ru-KNH}_2/\text{GNP}$ and Ru/GNP samples were loaded in an air-tight sample holder inside an Ar glovebox to avoid air exposure during measurements. All of the measurements were conducted at room temperature.

2.4. Catalyst Testing. Ammonia decomposition activity tests in a 10% $\text{NH}_3\text{-He}$ flow were performed in a

Micromeritics AutoChem II setup coupled with a Hiden mass spectroscopy (MS). Typically, 100 mg sample was placed in the center of a quartz reactor and tested under a flow of 10% NH_3/He (25 mL min^{-1}) at ambient pressure. The gases were analyzed using the Hiden QIC mass analyzer to follow the change of concentrations of NH_3 , H_2 , and N_2 in the stream. Ammonia decomposition activity tests in a pure NH_3 flow were performed in a continuous flow fixed-bed quartz reactor at the Dalian Institute of Chemical Physics. The gas composition was analyzed using online gas chromatograph (GC-2014C, Shimadzu) equipped with a Porapak N column, a 5A molecular sieve column, and a TCD detector. As an example, an MS profile and a GC profile for production analysis are shown in Figure S1. The error and reproducibility for NH_3 conversion at each temperature were within 5%. The method for determining apparent activation energy (E_a) of different catalysts is described in the Supporting Information. The conversion level was kept below 30% to make sure that the measurement conditions were far from thermodynamic equilibrium.

3. RESULTS AND DISCUSSION

3.1. Structural Characterization. In this section, the as-prepared samples were investigated by a series of characterization methods. Figure 1a shows the X-ray diffraction (XRD)

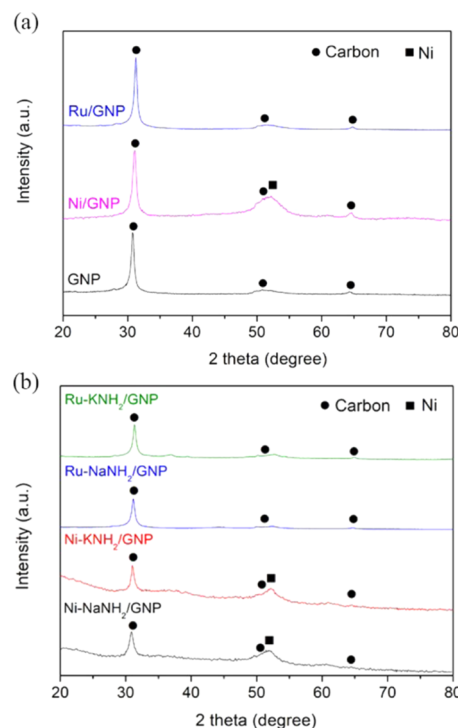


Figure 1. XRD patterns for (a) the carbon support (GNP) with or without Ni or Ru, and (b) Ni- or Ru-doped alkali metal amide nanocomposites. Each pattern is normalized to the main carbon peak in each sample.

patterns of the carbon support with and without transition metals. The diffraction peaks of GNP at 31° , 52° , and 64° correspond to the lattice planes (002), (100), and (004) of graphitic carbon. After addition of the Ni, a broad peak was observed around 53° in the sample Ni/GNP , mostly overlapping with one of the diffraction peaks of the graphitic carbon, which is ascribed to the (100) reflection of Ni. For the

Ru/GNP, diffraction peaks of Ru were not observed because of the low Ru loading (0.8 wt %). As a result, the crystallite sizes of Ni or Ru in the samples cannot be determined from the XRD patterns. However, we will show later by electron microscopy that not only Ni but also Ru nanoparticles were indeed present on the carbon support. The sharp diffraction peaks of NaNH_2 or KNH_2 were clearly seen from the physical mixtures with NaNH_2 or KNH_2 added, which indicates that in this case, large crystallites of NaNH_2 or KNH_2 are present (Figure S2). Figure 1b shows the XRD patterns of Ni- or Ru-doped amide nanocomposites. Interestingly, after melt infiltration with NaNH_2 or KNH_2 , only carbon and Ni diffraction peaks were observed, indicating the absence of crystalline NaNH_2 or KNH_2 in the nanocomposites.

N_2 physisorption measurements were performed on the nanocomposites, as well as the carbon support both with and without transition metals (Figure S3). An overview of the textural properties extracted from N_2 physisorption is given in Table 2. The deposition of Ni or Ru led to a slight decrease of

Table 2. Summary of Data Determined from Nitrogen Physisorption for GNP, GNP-Supported Ni or Ru, and the Nanocomposites^a

samples	BET surface area ($\text{m}^2 \text{g}^{-1}$)	micropore volume ($\text{cm}^3 \text{g}^{-1}$)	mesopore volume ($\text{cm}^3 \text{g}^{-1}$)	pore volume loss ($\text{cm}^3 \text{g}^{-1}$)
GNP	494	0.06	0.70	
Ni/GNP	392	0.06	0.49	
Ru/GNP	491	0.06	0.62	
Ni- NaNH_2 /GNP	159	0.00	0.42	0.13 ^(a)
Ni- KNH_2 /GNP	108	0.01	0.40	0.14 ^(a)
Ru- NaNH_2 /GNP	248	0.02	0.54	0.12 ^(b)
Ru- KNH_2 /GNP	167	0.02	0.44	0.22 ^(b)

^aAll of the data were calculated based on per gram carbon support. The value of pore volume loss of each sample was calculated by subtracting the total pore volume of the nanocomposite from that of Ni/GNP (a) or of Ru/GNP (b).

both the specific surface area and the pore volumes of GNP. Addition of amides in a physical mixture did not significantly change the pore volume of the carbon materials (Table S1). However, upon melt infiltration with NaNH_2 or KNH_2 , a significant loss of pore volume was observed.

Figure 2 illustrates the changes in textural properties upon the formation of the Ni- NaNH_2 /GNP nanocomposite. The pores of the GNP support were predominantly smaller than 10 nm with a continuous distribution up to ca. 50 nm. A lowering of the overall pore volume but little change in the pore size distribution was observed upon Ni deposition. Infiltrating NaNH_2 caused a loss specifically of the pores of 10 nm and smaller. When comparing the pore size distribution before and after adding NaNH_2 , the lost pore volume can be assumed to represent the volume of NaNH_2 in the pores. In this way, the particle size distribution of the NaNH_2 confined to the pores can therefore be roughly estimated by subtracting the pore size distribution of the nanocomposite from that of Ni/GNP. The resulting distribution of pore volume loss (green line in Figure 2) suggests that NaNH_2 occupies preferentially pores up to 10 nm. The total pore volume loss ($0.13 \text{ cm}^3 \text{g}^{-1}$) of the carbon support of the nanocomposite is almost equal to the volume ($0.14 \text{ cm}^3 \text{g}^{-1}$) of NaNH_2 added (Table S2), suggesting that the NaNH_2 resides inside the pores of the scaffold.

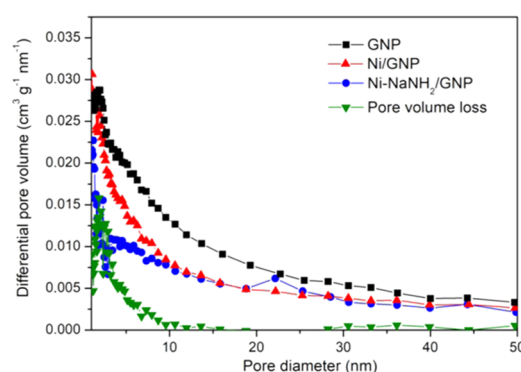


Figure 2. Pore size distributions obtained from nitrogen physisorption measurements for carbon support, Ni/GNP, and the Ni- NaNH_2 /GNP nanocomposite. Differential pore volumes were calculated per gram carbon support. The distribution of pore volume loss (green curve) was calculated by subtracting the pore size distribution of the Ni- NaNH_2 /GNP nanocomposite from that of Ni/GNP.

Similar distributions of pore volume loss were obtained for the other nanocomposites such as Ni- NaNH_2 /GNP, Ru- NaNH_2 /GNP, and Ru- KNH_2 /GNP, suggesting that the vast majority of NaNH_2 and KNH_2 were incorporated into pores with a size of up to 10 nm (Figures S4 and S5). Therefore, it can be concluded that the NaNH_2 and KNH_2 were successfully confined in the pores of the carbon support by melt infiltration.

As crystallite size determination from XRD was hampered by the overlap of diffraction peaks, the Ni particle size distribution of the nanocomposites was investigated by transmission electron microscopy (TEM), as shown in Figure 3. Ni particles with average sizes of 5.4 and 5.7 nm were observed in Ni- NaNH_2 /GNP and Ni- KNH_2 /GNP, respectively, similarly sizes as the Ni particles in the parent Ni/GNP. Hence, the melt infiltration process did not change the particle size of Ni. Scanning electron microscopy (SEM) and energy-dispersive X-ray spectrometry (EDX) were applied to obtain an insight into the morphology and element distributions of the samples (Figure 4). From the SEM images, a typical morphology of graphite is observed, and no particles were found on the outer surface of the support. EDX mapping gave the distributions of Ni, Na, and K in the same area of the samples. Ni, Na, and K distributions resemble that for carbon, indicating that the Ni and amide species were highly dispersed on the carbon support.

Ru-doped nanocomposites were characterized by high-angle annular dark-field scanning transmission electron microscopy (HAADF-STEM) and energy-dispersive X-ray spectrometry (EDX). As displayed in Figure 5, EDX mapping indicates that Na and K were distributed throughout the carbon support, and the Ru particles were uniformly distributed over the carbon support of both nanocomposites as evidenced by the bright spots in the dark-field images. The mean sizes of Ru in Ru- NaNH_2 /GNP and Ru- KNH_2 /GNP were 3.4 and 4.0 nm, respectively, similar to that of Ru/GNP itself. Additionally, it can be clearly seen from the Na and K maps that their location overlaps with that of Ru, suggesting nanoscale intimacy between Ru and amide species.

3.2. Catalytic Decomposition of Ammonia. Ammonia decomposition in the presence of the nanocomposite catalysts as well as in the presence of reference catalysts was performed under a flow of 10% NH_3 in He with a gas hourly space

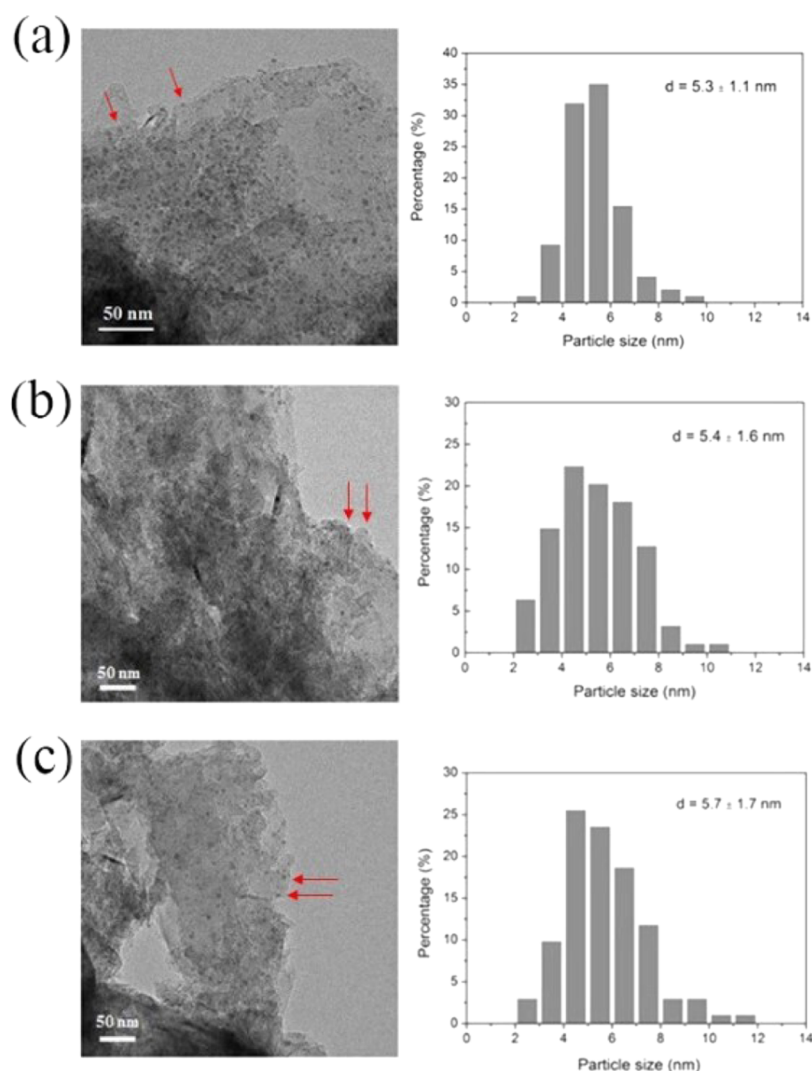


Figure 3. Representative TEM images and particle size distributions of the nanocomposites (a) Ni/GNP, (b) Ni-NaNH₂/GNP, and (c) Ni-KNH₂/GNP. Red arrows indicate Ni particles.

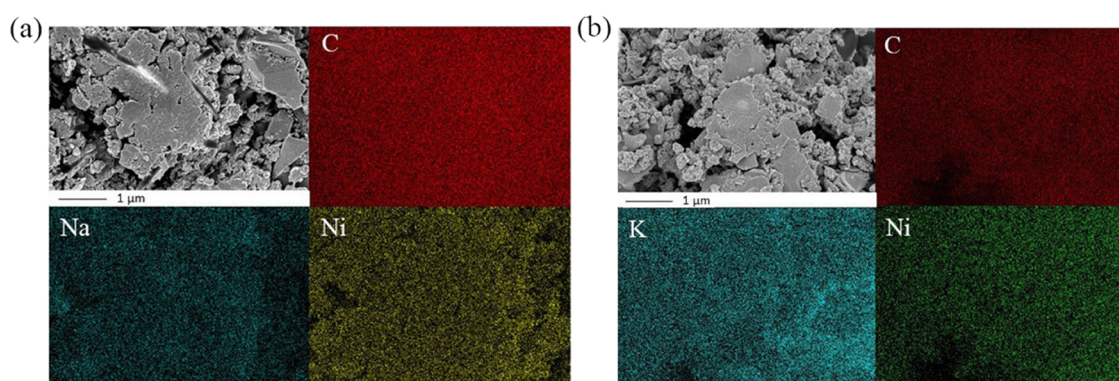


Figure 4. SEM images and EDX mapping of the nanocomposites (a) Ni-NaNH₂/GNP and (b) Ni-KNH₂/GNP.

velocity of 12000 h⁻¹. Macrocrystalline NaNH₂ or KNH₂ and their nanocomposites without transition metals show negligible ammonia conversion (less than 10% at 500 °C, see Figures S6 and S7). As shown in Figure 6, Ni/GNP led to 2% conversion at 300 °C, 11% conversion at 350 °C, and 28% conversion at 400 °C. The NH₃ conversions over the physical mixtures were similar to that of Ni/GNP only (Figure S8). Interestingly, the Ni-doped nanocomposites exhibited 3–5 times higher

activities over the whole temperature range tested. Similarly, Ni-KNH₂/GNP gives much higher activities than Ni/GNP. Up to 450 °C, the conversions were even comparable to that of Ru/GNP.

Decreasing NH₃ conversion was observed when the temperature was raised above 450 °C, and additional stability tests at selected temperatures were conducted (Figure S9). Similar activity losses were observed in previously reported

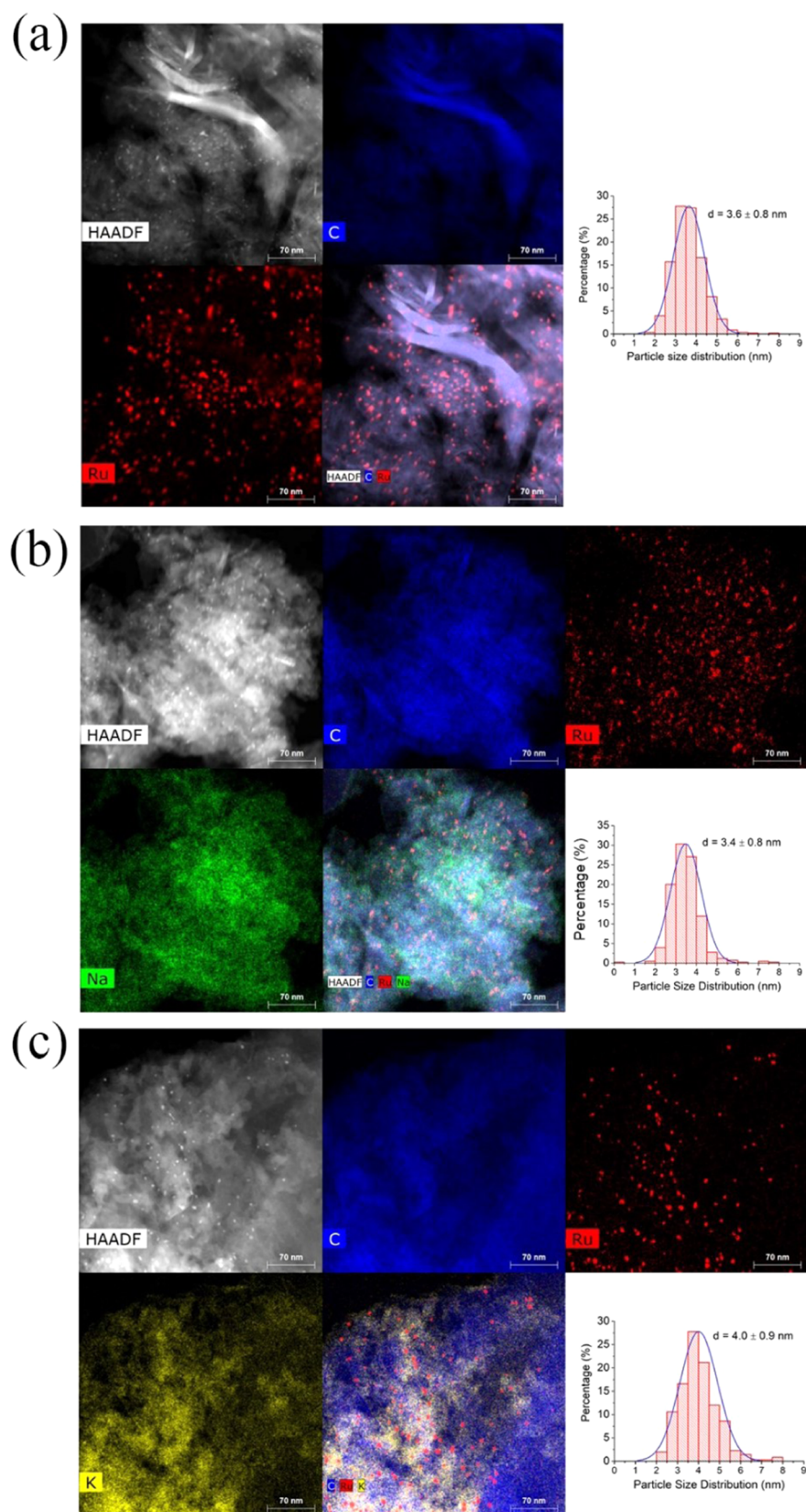


Figure 5. Representative HAADF-STEM images, EDX mapping (C blue, Ru red, Na green, and K yellow) and Ru particle size distributions for the nanocomposites (a) Ru/GNP, (b) Ru-NaNH₂/GNP, and (c) Ru-KNH₂/GNP.

amide-based catalysts and this was attributed to the loss of NaNH₂ and KNH₂ species due to their volatility at high temperatures.^{27,29,30} We therefore investigated the thermal

stability of our catalysts by performing TGA on the Ni-NaNH₂/GNP and Ni-KNH₂/GNP in an argon flow (Figure S10). Both samples started to lose weight upon heating and

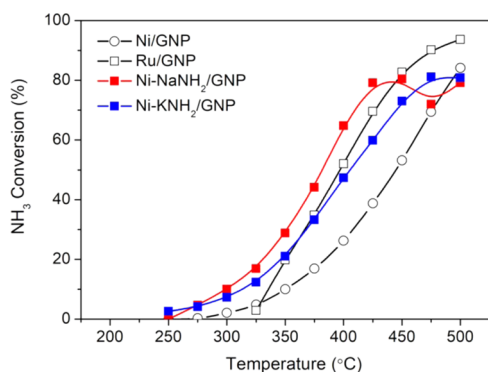


Figure 6. Ammonia conversion of the nanocomposites Ni-NaNH₂/GNP and Ni-KNH₂/GNP and the reference catalysts Ni/GNP and Ru/GNP in the temperature range of 250–500 °C. Reaction conditions: catalyst loading – 100 mg, 10% NH₃/He flow rate – 25 mL min^{−1}.

had a weight loss of about 1.6–4 wt % at 400 °C with a ramp rate of 5 °C min^{−1}. This indicates that only a small part of NaNH₂ and KNH₂ (8–20%) in the catalysts was lost upon heating, thus showing improved thermal stability. Although NaNH₂ and KNH₂ have relatively low melting points (210 and 330 °C respectively), it is likely that evaporation is limited by the encapsulation of amides in the porous carbon matrix, and their favorable interaction (wetting) with the carbon material. Deactivation of our catalysts at high temperatures could also be caused by a reaction between carbon and amides, forming, for instance, inactive cyanamides.³³ However, no crystalline NaCN or KCN phase was observed using XRD, suggesting that the decomposition product, if formed, was amorphous. Exploring other promising supports such as a metal oxide or porous silica to confine alkali metal amide catalysts could be an effective way to eliminate the formation of cyanamides and thus improve the stability in further study. Also, both XRD and TEM results did not show a significant change in the structure/morphology of the carbon after the catalytic tests.

The ammonia conversions of Ru-doped nanocomposites and reference catalysts are given in Figure 7. Ru/GNP decomposes NH₃ at 325 °C and above. NaOH- or KOH-promoted Ru/GNP catalysts presented improved activities, especially in the temperature range of 250–425 °C. Interestingly, Ru-NaNH₂/

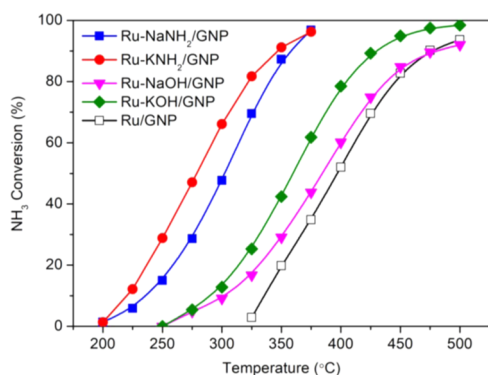


Figure 7. Ammonia conversion of the nanocomposites Ru-NaNH₂/GNP and Ru-KNH₂/GNP, the reference catalysts Ru/GNP and NaOH- or KOH-promoted Ru/GNP in the temperature range of 200–500 °C. Reaction conditions: catalyst loading – 100 mg, 10% NH₃/He flow rate – 25 mL min^{−1}. NH₃ conversion was recorded after a duration of 1.5 h upon reaching each reaction temperature.

GNP and Ru-KNH₂/GNP exhibited significant activities at temperatures as low as 200 °C, and their NH₃ conversions below 300 °C were 1 order of magnitude higher than for alkali hydroxide promoted Ru/GNP. Both Ru-doped nanocomposites led to near full conversion at 375 °C, 100 °C lower than for NaOH- or KOH-promoted Ru/GNP catalysts. Under the same conditions, NH₃ conversion is higher over Ru-KNH₂/GNP than over Ru-NaNH₂/GNP, indicating a slightly more effective promotion by KNH₂ for Ru. For the Ru-doped nanocomposite, gradual loss of activity was observed when being tested at 325 °C for 700 min (Figure S11). TGA of the Ru-NaNH₂/GNP and Ru-KNH₂/GNP are shown in Figure S10. As explained above, the reason for deactivation is probably slow reaction with the carbon support or some volatility of the compounds despite the protection by the carbon matrix.

It is also interesting to study the effects of the transition metal and amide loadings on the ammonia conversion, especially as the loadings have an influence on the contact between amides and transition metals. Figure 8a,b shows the influence of Ru loadings on the ammonia conversion of the nanocomposites at different temperatures. The conversion of ammonia increased on increasing Ru loadings from 0.1 to 1.6 wt %. A further increase in Ru loading did not change the activity significantly. It was reported that 3–5 nm Ru catalysts exhibited the best ammonia decomposition performance, which was attributed to the presence of abundant B5 sites.^{6,8,9} Our 0.8 wt % Ru-doped nanocomposites had an average particle size of 3–4 nm, as demonstrated by HAADF-STEM in Figure 5. Figure 8c,d shows the influence of NaNH₂ or KNH₂ loadings on the ammonia conversion of the nanocomposites at different temperatures. The nanocomposites with amide loadings of 5 and 10 wt % exhibited conversions of 10% or less even at 350 °C. The maximum conversions were achieved for the catalysts with an amide loading of 20%. The ammonia conversion decreased when the loading was increased to 30%, which can be explained by the presence of large amides crystals in the nanocomposites (Figure S12) which hinder the effective contact between Ru and amides inside the pores of the carbon support.

To explore high hydrogen production rates, the catalytic performance of Ni- and Ru-doped amide nanocomposites was also evaluated in a pure NH₃ flow (Figure S13). The influence of space velocity on NH₃ conversion is shown in Figure S14 for the Ru-NaNH₂/GNP catalyst as an example. Ammonia decomposition activities of different catalysts in a pure NH₃ flow are compared in Table S3. Under the same reaction conditions, the hydrogen formation rates of the Ni-NaNH₂/GNP and Ni-KNH₂/GNP are 3.7 and 2.9 times higher than that of the Ni-Li₂NH catalyst, respectively. The hydrogen formation rates of Ru-NaNH₂/GNP and Ru-KNH₂/GNP were about 5 times higher than that of the state-of-the-art catalyst Ru/CNTs, and 3.9 and 3.3 times higher than that of the reported Ru-Li₂NH/MgO. These results confirm the outstanding performance of our transition metal-doped amide nanocomposites.

3.3. Activation Energies and Possible Catalytic Mechanism. Figure 9 compares the Arrhenius plots for the different catalysts derived from the ammonia conversion curves. The apparent activation energies (E_a) of Ni/GNP and Ru/GNP are 86.1 and 73.2 kJ mol^{−1}, respectively, consistent with the values reported in the literature for traditional Ni- or Ru-based catalysts (Table 3). Interestingly,

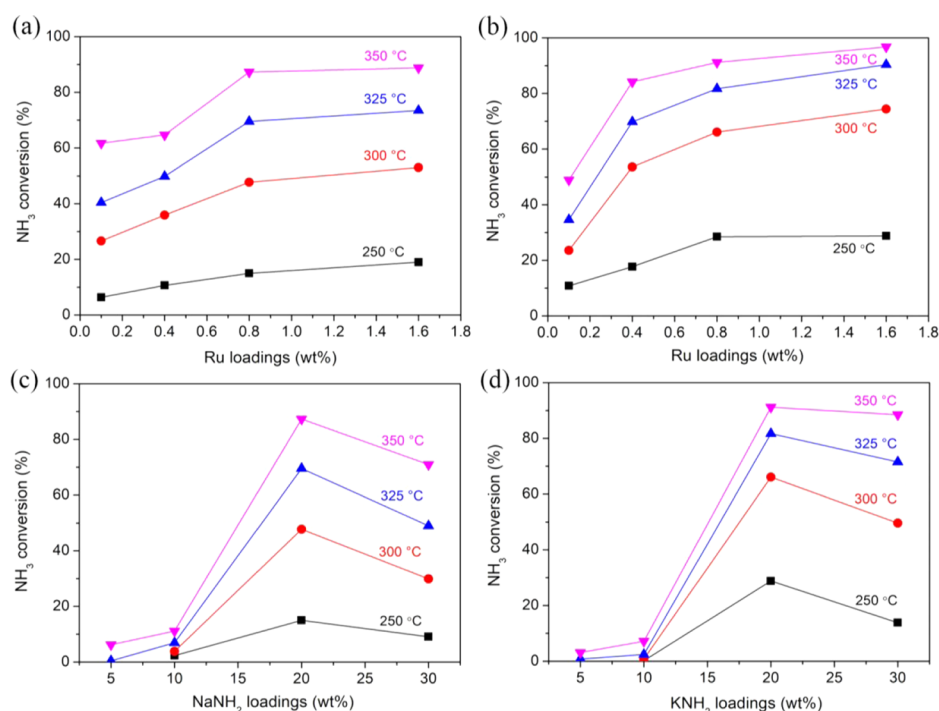


Figure 8. Influence of Ru loading on the ammonia conversion at selected temperatures for the Ru-NaNH₂/GNP nanocomposite (a) and the Ru-KNH₂/GNP nanocomposite (b). Influence of NaNH₂ or KNH₂ loading on the ammonia conversion at selected temperatures for the Ru-NaNH₂/GNP nanocomposite (c) and Ru-KNH₂/GNP nanocomposite (d). Reaction conditions: catalyst loading – 100 mg, 10% NH₃/He flow rate – 25 mL min⁻¹.

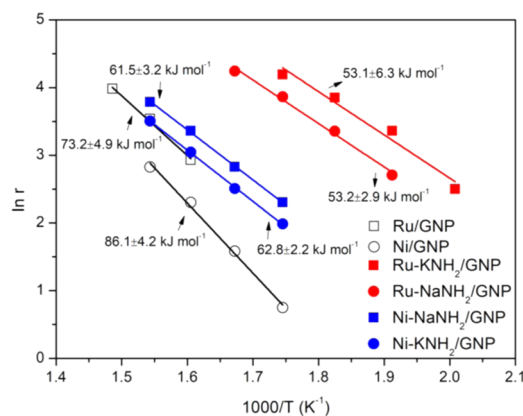


Figure 9. Arrhenius plots and apparent activation energies of the nanocomposite catalysts and reference catalysts. The uncertainty of activation energies given is only the error of linear fit of Arrhenius plots.

Table 3. Apparent Activation Energies of Various Catalysts

category	catalyst	E_a (kJ mol ⁻¹)	reference
Ni-based catalysts	Ni/GNP	86.1	this work
	Ni-NaNH ₂ /GNP	61.5	this work
	Ni-KNH ₂ /GNP	62.8	this work
	Ni/SiO ₂	108	35
	Ni/CNTs	90.3	19
Ru-based catalysts	Ru/GNP	73.2	this work
	Ru-NaNH ₂ /GNP	53.2	this work
	Ru-KNH ₂ /GNP	53.1	this work
	Ru/CNTs	69.2	36
	Ru/C12A7:e ⁻	54.9	37
	Ru-LiNH ₂ /MgO	53.2	30

the activation barriers for the Ni- or Ru-doped nanocomposites are in the range of only 53.1–62.8 kJ mol⁻¹, among the lowest values for ammonia decomposition catalysts reported in the literature. It can be concluded that the close contact between transition metals and pore-confined amide species in the nanocomposites results in greatly decreased kinetic barriers, independent of the exact amide, and excellent performance in the decomposition of ammonia.

To gain insight into the possible reaction mechanism, we conducted XAS measurements on the Ru K-edge of the Ru-KNH₂/C nanocomposite (Figure S15). The preliminary results show that the absorption edge for Ru-KNH₂ increases by ca. 2 eV compared to Ru foil and Ru/C. This indicates that Ru in the Ru-KNH₂ sample has a higher oxidation state than metallic Ru. Such an increase in oxidation state has been reported for other TM-amide-based catalysts, and was attributed to charge transfer between Ru and KNH₂ to form Ru-N bonds (or ternary nitride species) and thereby catalyzing the decomposition of NH₃.³⁸ For example, it has been reported that NH₃ decomposition over Li₂NH doped with 3d transition metals (nitrides) such as Fe, Co, and MnN involve two steps:²⁸ (1) the reaction of Li₂NH and transition metal (nitride) to form ternary nitride and H₂; (2) the ammoniation of the ternary nitride to Li₂NH, transition metal (nitride), and N₂. Ternary nitride is not expected to be formed in systems such as Ru-Li₂NH, MnN-NaNH₂, and MnN-KNH₂. Likewise, ternary nitrides such as Na-Ni-N, K-Ni-N, Na-Ru-N, and K-Ru-N have not been reported. Nevertheless, recent results from Guo et al. suggest that Ru interacts with NH_x of Li₂NH, as evidenced by a similar increase in the oxidation state of Ru. The authors suggested that the interaction destabilizes/decreases the strong repulsion between the negative charged NH_x ($x = 1, 2$), thereby

facilitating partial decomposition of the amide and reaction with NH_3 to produce N_2 and H_2 under NH_3 .^{30,39} The exact nature of the interaction between Ru and amides is a subject of further investigation, but the current results strongly suggest that the catalytic mechanism of our catalysts is similar to that reported for TM-amide catalysts prepared by ball milling. However, the very close proximity between the amide and transition metal upon nanoconfinement, enhances the interaction, leading to a much higher catalytic activity than for the ball-milled samples.

4. CONCLUSIONS

In conclusion, we prepared pore-confined NaNH_2 and KNH_2 nanocomposites by melt infiltration. NaNH_2 and KNH_2 were successfully embedded inside the pores of the carbon support with a particle size distribution of 2–10 nm. Ni- and Ru-doped nanocomposites show promising ammonia decomposition activity. The hydrogen production rates of Ni- and Ru-doped nanocomposites were about 3–4 times higher than for the state-of-the-art amide-based catalysts, such as Ni– Li_2NH and Ru– $\text{Li}_2\text{NH}/\text{MgO}$. This study shows that nanosizing of alkali metal amides via pore confinement improves the interfacial contact between amides and transition metals, leading to much decreased kinetic barriers for ammonia decomposition. Pore confinement of alkali metal amides provides a promising way to effectively generate H_2 from NH_3 at low temperatures.

■ ASSOCIATED CONTENT

Supporting Information

The Supporting Information is available free of charge on the ACS Publications website at DOI: 10.1021/acs.jpcc.9b03878.

Additional experimental data including: determination of the apparent activation energy; textural properties of the physical mixtures; amide volume and pore volume loss of amide nanocomposites; ammonia decomposition activity comparison under a flow of pure NH_3 ; GC and MS profiles for product analysis; XRD patterns of the physical mixtures; N_2 physisorption isotherms of various samples; particle size distributions of NaNH_2 and KNH_2 in the nanocomposites; the ammonia conversion profile of the blank reactor and macrocrystalline NaNH_2 and KNH_2 ; the ammonia conversion profile of the nanocomposites NaNH_2/GNP and KNH_2/GNP ; the ammonia conversion profile of the physical mixtures Ni/GNP– NaNH_2 –PM and Ni/GNP– KNH_2 –PM; catalytic stability of the nanocomposites; TGA measurements of the nanocomposites; XRD of the nanocomposites with an amide loading of 30 wt %; ammonia conversion of the nanocomposite catalysts under a pure NH_3 flow; influence of the pure NH_3 flow rate on NH_3 conversion of the Ru– NaNH_2/GNP ; XAS measurements of the Ru– KNH_2/GNP nanocomposite (PDF)

■ AUTHOR INFORMATION

Corresponding Authors

*E-mail: P.Ngene@uu.nl (P.N.).

*E-mail: P.E.dejongh@uu.nl (P.E.d.J.).

ORCID

Jianping Guo: 0000-0002-0229-8555

Peter Ngene: 0000-0003-3691-0623

Petra E. de Jongh: 0000-0002-2216-2620

Notes

The authors declare no competing financial interest.

■ ACKNOWLEDGMENTS

The authors would like to acknowledge Sander Lambregts for N_2 physisorption measurements, Lisette Pompe for TEM measurements, Jochem Wijten for SEM–EDX measurements, Wouter Lamme for STEM–EDX measurements, and Thomas Hartman for Raman spectroscopy measurements, as well as Marjan Versluis and Jan-Willem de Rijk for technical support. The authors would also like to thank the NWO-Vici (16.130.344) for overall funding of the project. P.N. and P.E.d.J. acknowledge support from the European Research Council (ERC) under the European Union's Horizon 2020 research and innovation program (ERC-2014-CoG No 648991). J.G. thanks the financial support from the National Natural Science Foundation of China (Grant No. 21872137). We thank Prof. Ping Chen for the fruitful discussion. We acknowledge the Dutch-Belgian beamline (DUBBLE) at the European Synchrotron Radiation Facility (ESRF) for providing synchrotron radiation facilities (proposal number 26-01-1171). Alessandro Longo at ESRF is acknowledged for technical support.

■ ABBREVIATIONS

XRD, X-ray diffraction; SEM, scanning electron microscopy; TEM, transmission electron microscopy; HAADF-STEM, high-angle annular dark-field scanning transmission electron microscopy; EDX, energy-dispersive X-ray spectroscopy; MS, mass spectrometry; GC, gas chromatography; XAS, X-ray adsorption spectroscopy; TGA, thermogravimetric analysis; GNP, graphite nanoplatelet with a specific surface area ca. $500 \text{ m}^2 \text{ g}^{-1}$

■ REFERENCES

- (1) Grochala, W.; Edwards, P. P. Thermal Decomposition of the Non-interstitial Hydrides for the Storage and Production of Hydrogen. *Chem. Rev.* **2004**, *104*, 1283–1315.
- (2) He, T.; Pachfule, P.; Wu, H.; Xu, Q.; Chen, P. Hydrogen Carriers. *Nat. Rev. Mater.* **2016**, *1*, No. 16059.
- (3) Orimo, S. I.; Nakamori, Y.; Eliseo, J. R.; Zuttel, A.; Jensen, C. M. Complex Hydrides for Hydrogen Storage. *Chem. Rev.* **2007**, *107*, 4111–4132.
- (4) Eberle, U.; Felderhoff, M.; Schuth, F. Chemical and Physical Solutions for Hydrogen Storage. *Angew. Chem., Int. Ed.* **2009**, *48*, 6608–6630.
- (5) Klerke, A.; Christensen, C. H.; Norskov, J. K.; Vegge, T. Ammonia for Hydrogen Storage: Challenges and Opportunities. *J. Mater. Chem.* **2008**, *18*, 2304–2310.
- (6) Schüth, F.; Palkovits, R.; Schlögl, R.; Su, D. S. Ammonia as a Possible Element in an Energy Infrastructure: Catalysts for Ammonia Decomposition. *Energy Environ. Sci.* **2012**, *5*, 6278–6289.
- (7) Guo, J. P.; Chen, P. Catalyst: NH_3 as an Energy Carrier. *Chem* **2017**, *3*, 709–712.
- (8) Yin, S. F.; Xu, B. Q.; Zhou, X. P.; Au, C. T. A Mini-Review on Ammonia Decomposition Catalysts for On-Site Generation of Hydrogen for Fuel Cell Applications. *Appl. Catal., A* **2004**, *277*, 1–9.
- (9) García-Bordejé, E.; Armenise, S.; Roldan, L. Toward Practical Application of H_2 Generation From Ammonia Decomposition Guided by Rational Catalyst Design. *Catal. Rev.* **2014**, *56*, 220–237.
- (10) Mukherjee, S.; Devaguptapu, S. V.; Sviripa, A.; Lund, C. R. F.; Wu, G. Low-Temperature Ammonia Decomposition Catalysts for Hydrogen Generation. *Appl. Catal., B* **2018**, *226*, 162–181.
- (11) Lu, A. H.; Nitz, J. J.; Comotti, M.; Weidenthaler, C.; Schlichte, K.; Lehmann, C. W.; Terasaki, O.; Schuth, F. Spatially and Size

Selective Synthesis of Fe-Based Nanoparticles on Ordered Mesoporous Supports as Highly Active and Stable Catalysts for Ammonia Decomposition. *J. Am. Chem. Soc.* **2010**, *132*, 14152–14162.

(12) Zhang, J.; Muller, J. O.; Zheng, W. Q.; Wang, D.; Su, D. S.; Schlogl, R. Individual Fe-Co Alloy Nanoparticles on Carbon Nanotubes: Structural and Catalytic Properties. *Nano Lett.* **2008**, *8*, 2738–2743.

(13) Zheng, W. Q.; Cotter, T. P.; Kaghazchi, P.; Jacob, T.; Frank, B.; Schlichte, K.; Zhang, W.; Su, D. S.; Schuth, F.; Schlogl, R. Experimental and Theoretical Investigation of Molybdenum Carbide and Nitride as Catalysts for Ammonia Decomposition. *J. Am. Chem. Soc.* **2013**, *135*, 3458–3464.

(14) Simonsen, S. B.; Chakraborty, D.; Chorkendorff, I.; Dahl, S. Alloyed Ni-Fe Nanoparticles as Catalysts for NH_3 Decomposition. *Appl. Catal., A* **2012**, *447–448*, 22–31.

(15) Choi, J. G. Ammonia Decomposition over Vanadium Carbide Catalysts. *J. Catal.* **1999**, *182*, 104–116.

(16) Bell, T. E.; Torrente-Murciano, L. H_2 Production via Ammonia Decomposition Using Non-Noble Metal Catalysts: A Review. *Top Catal.* **2016**, *59*, 1438–1457.

(17) Pelka, R.; Kielbasa, K.; Arabczyk, W. Catalytic Ammonia Decomposition during Nanocrystalline Iron Nitriding at 475 °C with NH_3/H_2 Mixtures of Different Nitriding Potentials. *J. Phys. Chem. C* **2014**, *118*, 6178–6185.

(18) Tagliazucca, V.; Schlichte, K.; Schuth, F.; Weidenthaler, C. Molybdenum-based Catalysts for the Decomposition of Ammonia: In situ X-ray Diffraction Studies, Microstructure, and Catalytic Properties. *J. Catal.* **2013**, *305*, 277–289.

(19) Yin, S. F.; Zhang, Q. H.; Xu, B. Q.; Zhu, W. X.; Ng, C. F.; Au, C. T. Investigation on the Catalysis of CO_x -Free Hydrogen Generation from Ammonia. *J. Catal.* **2004**, *224*, 384–396.

(20) García-García, F. R.; Alvarez-Rodriguez, J.; Rodriguez-Ramos, I.; Guerrero-Ruiz, A. The Use of Carbon Nanotubes with and without Nitrogen Doping as Support for Ruthenium Catalysts in the Ammonia Decomposition Reaction. *Carbon* **2010**, *48*, 267–276.

(21) Armenise, S.; Roldan, L.; Marco, Y.; Monzon, A.; Garcia-Bordeje, E. Elucidation of Catalyst Support Effect for NH_3 Decomposition Using Ru Nanoparticles on Nitrogen-Functionalized Carbon Nanofiber Monoliths. *J. Phys. Chem. C* **2012**, *116*, 26385–26395.

(22) Ertl, G.; Weiss, M.; Lee, S. B. Role of Potassium in the Catalytic Synthesis of Ammonia. *Chem. Phys. Lett.* **1979**, *60*, 391–394.

(23) Strongin, D. R.; Somorjai, G. A. The Effects of Potassium on Ammonia-Synthesis over Iron Single-Crystal Surfaces. *J. Catal.* **1988**, *109*, 51–60.

(24) Hansgen, D. A.; Vlachos, D. G.; Chen, J. G. G. Using First Principles to Predict Bimetallic Catalysts for the Ammonia Decomposition Reaction. *Nat. Chem.* **2010**, *2*, 484–489.

(25) Guo, W.; Vlachos, D. G. Patched Bimetallic Surfaces are Active Catalysts for Ammonia Decomposition. *Nat. Commun.* **2015**, *6*, No. 8619.

(26) Titherley, A. W. XLV.-Sodium, Potassium, and Lithium amides. *J. Chem. Soc., Trans.* **1894**, *65*, 504–522.

(27) David, W. I. F.; Makepeace, J. W.; Callear, S. K.; Hunter, H. M. A.; Taylor, J. D.; Wood, T. J.; Jones, M. O. Hydrogen Production from Ammonia Using Sodium Amide. *J. Am. Chem. Soc.* **2014**, *136*, 13082–13085.

(28) Guo, J. P.; Wang, P. K.; Wu, G. T.; Wu, A. A.; Hu, D. Q.; Xiong, Z. T.; Wang, J. H.; Yu, P.; Chang, F.; Chen, Z.; et al. Lithium Imide Synergy with 3d Transition-Metal Nitrides Leading to Unprecedented Catalytic Activities for Ammonia Decomposition. *Angew. Chem., Int. Ed.* **2015**, *54*, 2950–2954.

(29) Guo, J. P.; Chang, F.; Wang, P. K.; Hu, D. Q.; Yu, P.; Wu, G. T.; Xiong, Z. T.; Chen, P. Highly Active MnN- Li_2NH Composite Catalyst for Producing CO_x -Free Hydrogen. *ACS Catal.* **2015**, *5*, 2708–2713.

(30) Guo, J. P.; Chen, Z.; Wu, A. A.; Chang, F.; Wang, P. K.; Hu, D. Q.; Wu, G. T.; Xiong, Z. T.; Yu, P.; Chen, P. Electronic Promoter or

Reacting Species? The Role of LiNH_2 on Ru in Catalyzing NH_3 Decomposition. *Chem. Commun.* **2015**, *51*, 15161–15164.

(31) de Jongh, P. E.; Adelhelm, P. Nanosizing and Nanoconfinement: New Strategies Towards Meeting Hydrogen Storage Goals. *ChemSusChem* **2010**, *3*, 1332–1348.

(32) de Jongh, P. E.; Eggenhuisen, T. M. Melt Infiltration: an Emerging Technique for the Preparation of Novel Functional Nanostructured Materials. *Adv. Mater.* **2013**, *25*, 6672–6690.

(33) Bramwell, P. L.; Lentink, S.; Ngene, P.; de Jongh, P. E. Effect of Pore Confinement of LiNH_2 on Ammonia Decomposition Catalysis and the Storage of Hydrogen and Ammonia. *J. Phys. Chem. C* **2016**, *120*, 27212–27220.

(34) Wang, S. J.; Yin, S. F.; Li, L.; Xu, B. Q.; Ng, C. F.; Au, C. T. Investigation on Modification of Ru/CNTs Catalyst for the Generation of CO_x -Free Hydrogen from Ammonia. *Appl. Catal., B* **2004**, *52*, 287–299.

(35) Atsumi, R.; Noda, R.; Takagi, H.; Vecchione, L.; Di Carlo, A.; Del Prete, Z.; Kuramoto, K. Ammonia Decomposition Activity over Ni/SiO₂ Catalysts with Different Pore Diameters. *Int. J. Hydrogen Energ.* **2014**, *39*, 13954–13961.

(36) Yin, S. F.; Xu, B. Q.; Zhu, W. X.; Ng, C. F.; Zhou, X. P.; Au, C. T. Carbon Nanotubes-Supported Ru Catalyst for the Generation of CO_x -Free Hydrogen from Ammonia. *Catal. Today* **2004**, *93–95*, 27–38.

(37) Hayashi, F.; Toda, Y.; Kanie, Y.; Kitano, M.; Inoue, Y.; Yokoyama, T.; Hara, M.; Hosono, H. Ammonia Decomposition by Ruthenium Nanoparticles Loaded on Inorganic Electride C12A7:e(-). *Chem. Sci.* **2013**, *4*, 3124–3130.

(38) Kishida, K.; Kitano, M.; Inoue, Y.; Sasase, M.; Nakao, T.; Tada, T.; Abe, H.; Niwa, Y.; Yokoyama, T.; Hara, M.; et al. Large Oblate Hemispheroidal Ruthenium Particles Supported on Calcium Amide as Efficient Catalysts for Ammonia Decomposition. *Chem. - Eur. J.* **2018**, *24*, 7976–7984.

(39) Chang, F.; Guo, J. P.; Wu, G. T.; Wang, P. K.; Yu, P.; Chen, P. Influence of Alkali Metal Amides on the Catalytic Activity of Manganese Nitride for Ammonia Decomposition. *Catal. Today* **2017**, *286*, 141–146.